

r-Process enrichment in the Galactic halo characterized by nucleosynthesis variation
in the ejecta of coalescing neutron star binaries

TAKUJI TSUJIMOTO,¹ NOBUYA NISHIMURA,² AND KOUTAROU KYUTOKU^{3,2,4,5}

¹*National Astronomical Observatory of Japan, Mitaka, Tokyo 181-8588, Japan*

²*Center for Gravitational Physics, Yukawa Institute for Theoretical Physics, Kyoto University, Kyoto 606-8502, Japan*

³*Department of Physics, Kyoto University, Kyoto 606-8502, Japan*

⁴*Theory Center, Institute of Particle and Nuclear Studies, KEK, Tsukuba 305-0801, Japan*

⁵*Interdisciplinary Theoretical and Mathematical Sciences Program (iTHEMS), RIKEN, Wako, Saitama 351-0198, Japan*

(Received xxx; Revised xxx; Accepted xxx)

ABSTRACT

A large star-to-star variation in the abundances of r-process elements, as seen in the [Eu/Fe] ratio for Galactic halo stars, is a prominent feature that is distinguishable from other heavy elements. It is, in part, caused by the presence of highly r-process enriched stars, classified as r-II stars ([Eu/Fe] ≥ +1). In parallel, halo stars show that the ratio of a light r-process element (Y) to Eu is tightly correlated with [Eu/Fe], giving the lowest [Y/Eu] ratio that levels off at r-II stars. On the other hand, recent hydrodynamical simulations of coalescing double neutron stars (cNSNSs) have suggested that r-process sites may be separated into two classes providing different electron-fraction distributions: tidally-driven dynamical ejecta and (dynamical or postmerger) non-tidal ejecta. Here, we show that a widely spanning feature of [Eu/Fe] can be reproduced by models that consider the different masses of tidally-driven dynamical ejecta from both cNSNSs and coalescing black hole/neutron star binaries (cBHNSs). In addition, the observed [Y/Eu] trend is explained by the combined nucleosynthesis in two kinds of ejecta with varying mass asymmetry in double NS systems. Our scenario suggests that massive tidally-driven dynamical ejecta accompanied by massive non-tidal part from cNSNSs or cBHNSs could alone accommodate r-II abundances, including an actinide boost in some cases. The event rate for cNSNSs estimated from our study agrees with the latest result of ∼ 1000 (90% confidence interval of 110–3840) Gpc⁻³yr⁻¹ by gravitational-wave detection, and a few events per Gpc³ per year of cBHNSs associated with r-process production are predicted to emerge.

Keywords: Galaxy: halo — gravitational waves — nuclear reactions, nucleosynthesis, abundances — stars: abundances

1. INTRODUCTION

Clear answers to the origin and evolution of r-process elements continue to elude us, even after the discovery of gravitational waves from coalescing double neutron star (cNSNS) GW170817 and the subsequent discovery of multi-wavelength electromagnetic counterparts that identified cNSNSs as a promising major source of r-process elements (e.g., Coulter et al. 2017; Smartt et al. 2017; Pian et al. 2017; Cowperthwaite et al. 2017; Thielemann et al. 2017). The stellar record of r-process

abundances leaves open the question of whether cNSNSs are the sole (major) site of the r-process. This is exemplified by two arguments: that the r-process abundance features of very metal-poor stars invoke the contribution from some specific core-collapse supernovae (CCSNe), the so-called magneto-rotational SNe (e.g., Winteler et al. 2012; Wehmeyer et al. 2015; Nishimura et al. 2015), and that disk stars suggest enrichment by another rare CCSNe, collapsars, as the major site of the r-process (MacFadyen & Woosley 1999; Fujimoto et al. 2008; Siegel et al. 2019). However, it is not clear whether these specific CCSNe exist if we consider the propagation of strong-magnetic jets in the models for magneto-rotational SNe (Nishimura et al.

2017; Halevi & Mösta 2018; Mösta et al. 2018) and constraints from stellar abundances of halo stars on collapsars (Macias & Ramirez-Ruiz 2019).

A large scatter seen in the [Eu/Fe] ratio, spanning nearly three orders of magnitude among Galactic halo stars, is a feature unique to r-process elements and thus should be connected to r-process sites and their nucleosynthesis (e.g., Cowan et al. 2019); however, the origin of the scatter has yet to be identified. Among Eu-measured halo stars, special attention has been directed to those stars having highly enhanced Eu abundances, as high as [Eu/Fe] > +1. These have been classified as r-II stars (Beers & Christlieb 2005) since the discovery of the first r-II star, CS 22892-052 (Snedden et al. 1994). Recent first detection of r-II stars outside the Galaxy in an ultra-faint dwarf galaxy Reticulum II (Ret II, Ji et al. 2016) triggered one possible scenario for the origin of Galactic r-II stars; i.e., these stars are accreted from disrupted small satellite galaxies (Roederer et al. 2018; Brauer et al. 2019). However, as seen in their orbital property that about 70 % of r-II stars reside within the inner regions (< 13 kpc) of the Galactic halo (Roederer et al. 2018), we have no clear kinematic evidence for their accretion history. Alternatively, observations suggest the possibility that r-II stars differ from other stars in the nucleosynthesis condition of the associated r-process events. These r-II stars are likely to be born in an environment that is neutron-rich enough to produce an actinide (e.g., Th and U) boost for about one third of them (Mashonkina et al. 2014), although the conditions for the actinide production involve uncertainties, including the possibility that actinides could be populated at the not that low electron fraction (Y_e) (e.g., Lippuner et al. 2017).

There is another implication for the connection between the variation in [Eu/Fe] and the nucleosynthesis of r-process events. The abundance ratios of light r-process elements (Sr, Y, and Zr)¹ to Eu are correlated with [Eu/Fe] in the sense that [light r-process/Eu] is larger for smaller [Eu/Fe] (Montes et al. 2007; Tsujimoto & Shigeyama 2014a). We need to answer why r-II stars show the lowest [light r-process/Eu] ratio among halo stars.

An astrophysical site that is different for light r-process elements than for heavy ones including Eu,

¹ Although the s-process dominates these neutron-capture elements in the solar abundance pattern, we focus on the chemical enrichment in the Galactic halo where the r-process is the major source for these elements in this study. Therefore, light neutron-capture elements are hereafter referred to as light r-process elements.

has been proposed as the mechanism behind the variation in [light r-process/Eu] for individual stars (Montes et al. 2007; François et al. 2007). Possible candidates include regular CCSNe producing Fe together (Qian & Wasserburg 2007) through the neutrino-driven wind from the proto-NS (Arcones & Bliss 2014), electron-capture SNe (Kitaura et al. 2006; Wanajo et al. 2011), and magneto-rotational SNe (Nishimura et al. 2017). However, our understanding to date should be reexamined in response to recent numerical simulations for r-process nucleosynthesis in cNSNSs. The latest discovery of a signature of synthesized light r-process element (Sr) in the afterglow of GW170817 strengthens this necessity (Watson et al. 2019).

Currently, binary NSs are regarded as being capable of producing various kinds of ejecta during the coalescence. Tidal interaction could allow the NS material to be ejected without experiencing significant shock heating nor neutrino irradiation (e.g., Freiburghaus et al. 1999; Sekiguchi et al. 2016; Vincent et al. 2019), although recent simulations have reported a non-negligible influence of neutrinos on such ejecta (Radice et al. 2018). These tidal ejecta may keep low Y_e and contribute predominantly to the production of heavy r-process elements such as Eu. Dynamical interaction also produces the shock-heated ejecta, whose Y_e is suggested by some studies to be increased to the extent that Eu is no longer produced efficiently and instead light r-process elements such as Y are produced (e.g., Wanajo et al. 2014). Following these dynamical ejecta, the merger remnant drives post-merger mass ejection via various possible mechanisms (e.g., Metzger & Fernández 2014; Just et al. 2015; Siegel & Metzger 2018; Fujibayashi et al. 2018). In particular, Fujibayashi et al. (2018) find that the post-merger wind from the torus surrounding a massive NS, which is likely to be formed for typical cNSNS, is primarily characterized by moderate Y_e values and dominantly produces light r-process elements. These updated theoretical inputs of cNSNS may have high potential for altering the interpretation of [light r-process/Eu] variation.

A close connection between the star-to-star variation in r-process abundances and cNSNSs is also implied from the wide range of [Eu/Fe] ratios. The mass of dynamical ejecta is predicted to vary as widely as two orders of magnitude ($\sim 10^{-4} - 0.01 M_\odot$: Hotokezaka et al. 2013, $\sim 2 \times 10^{-4} - 0.02 M_\odot$: Bauswein et al. 2013), where the *tidally-driven component* increases as the mass asymmetry increases. Further, its mass range widens if we consider the contribution from coalescing black hole/neutron star binaries (cBHNSs); i.e., the mass of

dynamical ejecta from cBHNSs can become as massive as $\sim 0.1 M_{\odot}$ dominated completely by the tidal component (Kyutoku et al. 2015). As a result, the ejected Eu mass can differ by approximately three orders of magnitude according to the difference in the mass of its production site. Then, it turns out that the degree of variation in an Eu mass broadly coincides with that for the observed [Eu/Fe] ratios. Indeed, in the Draco dwarf galaxy, we identified two r-process events with enriched gases at levels that differ by more than one order of magnitude (Tsujiimoto et al. 2017a). These arguments suggest that enrichment driven by both cNSNSs and cBHNSs makes a fundamental feature of Galactic r-process abundance, including the early onset of the r-process at low metallicities (Wehmeyer et al. 2019).

2. NUCLEOSYNTHESIS IN TIDAL AND NON-TIDAL EJECTA

In this study, we boldly classify the ejecta components into the tidal and non-tidal ejecta, which are responsible for the synthesis of Eu and Y, respectively. Such a classification is possible since the production sites of Eu and Y inside the ejecta can be seen as discrete in terms of the Y_e value. To investigate the dependence of nucleosynthesis yields on Y_e , we perform a set of r-process calculations, using a nuclear reaction network code (Nishimura et al. 2016, 2017) and the simplified models of merger ejecta for cNSNSs and cBHNSs. We adopt the adiabatic free-expansion evolution (Freiburghaus et al. 1999; Farouqi et al. 2010; Wanajo 2018), of which the abundance evolution is determined by the initial Y_e value, entropy, and expansion velocity.

The results of nucleosynthesis calculations are shown in Figure 1, in which the mass fractions of Eu and Y are plotted as a function of Y_e . The mass fraction has a band between the minimum and maximum values for the varieties of entropy: $10\text{--}35 k_B \text{ baryon}^{-1}$ and expansion velocity: $0.05\text{--}0.3$ of the speed of light. These adopted values cover the reasonable range for merger conditions/ejecta suggested by Wanajo (2018). We see a clear separation of Eu and Y production depending on the value of Y_e . The deviation of the mass fractions of Eu and Y lies within a factor of ~ 2 for $Y_e < 0.3$. It suggests that the final abundance of Eu, which is a key element of the tidal ejecta, is primarily determined by Y_e while the Y abundance shows a bit more complexity of a dependence on other factors. In addition, the uncertainty of the nuclear physics input such as the mass model and fission treatment (Mendoza-Temis et al. 2015; Goriely 2015; Eichler et al. 2015; Côté et al. 2018; Vassh et al. 2019) affects calculated abundances of products such as

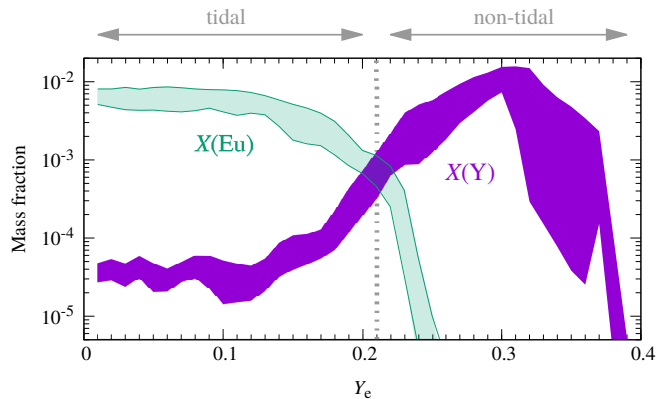


Figure 1. The mass fractions of Eu and Y by the r-process as a function of Y_e . The nucleosynthesis calculations (Nishimura et al. 2017) are performed with the parametric expansion model of merger ejecta (Wanajo 2018). The mass fraction has a band between the minimum and maximum values for the varieties of entropy: $10\text{--}35 k_B \text{ baryon}^{-1}$ and expansion velocity: $0.05\text{--}0.3$ of the speed of light. $Y_e \sim 0.22$ is the boundary of the tidal and non-tidal components assumed in this study.

Eu since dynamical ejecta conditions can synthesize nuclei well outside the reach of current experimental data.

We also need to keep in mind that the nucleosynthesis yields in both the dynamical and postmerger ejecta are inevitably dependent on many uncertain physics inputs in hydrodynamical simulations. Examples include neutrino transport scheme (Caballero et al. 2012; Foucart et al. 2016; Radice et al. 2018), neutrino oscillation (Malkus et al. 2016; Frensel et al. 2017; Tian et al. 2017), and neutron star equations of state (Sekiguchi et al. 2015; Bovard et al. 2017; Radice et al. 2018; Vincent et al. 2019). In particular, the r-process yields associated with the postmerger ejecta are critically important, because they could dominate the mass of ejecta in many cases, given the wide range of accretion disk mass ejection deduced (Côté et al. 2018). It is possible that the postmerger ejecta also efficiently produce Eu due to low Y_e if the BH is formed promptly after merger (Just et al. 2015; Siegel & Metzger 2018).

3. VARIATIONS IN [Eu/Fe] AND [Y/Eu]

We discuss more comprehensively the origin of variations in both [Eu/Fe] and [light r-process/Eu] and the correlation between the two. It was first found by Montes et al. (2007) that there exists a downward trend of [light r-process/Eu] with increasing [Eu/Fe] while [heavy r-process/Eu] stays constant with respect to [Eu/Fe] (here light r-process elements are Sr, Y and Zr and heavy ones include Ba, La, and Nd). This feature may suggest that the major source of light r-process el-

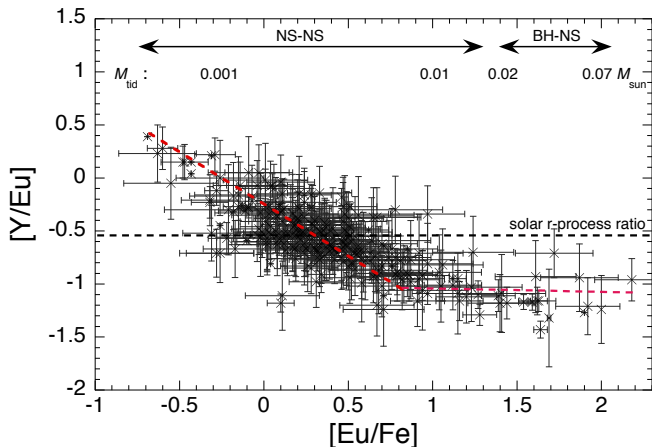


Figure 2. Observed correlation of $[Y/Eu]$ with $[Eu/Fe]$ for Galactic halo stars that reflect the r-process Y/Eu abundance ratio. The observed data are selected with $[Fe/H] < -2$ and $[Ba/Eu] < 0$ from a SAGA database (Suda et al. 2008). For r-II stars, the data are complemented by a JINA database (Abohalima & Frebel 2018). In addition, two r-II stars recently discovered (Sakari et al. 2018; Holmbeck et al. 2018) are also added. One extremely Eu-enhanced star ($[Eu/Fe] = +2.74$ and $[Y/Eu] = -0.84$; Allen et al. 2012) is not shown here. Black dashed line indicates the solar r-process ratio (Simmmerer et al. 2004; Bisterzo et al. 2014). Brief explanations are attached in the upper part (see the text). Here the assumed higher mass ejecta of low Y_e tidal ejecta for cBHNS scenarios is motivated by numerical simulation results (Kyutoku et al. 2015). Red dashed line indicates a mean abundance track.

elements is different from that of Eu (see also Aoki et al. 2005; François et al. 2007), and is proposed to be explained by the presence of a weak r-process producing source such as the light element primary process (LEPP) as a consequence of the correlation of light r-process elements with Fe instead of Eu (Travaglio et al. 2004; Montes et al. 2007).

With an update of the observational data, we revisit this matter using Y for light r-process elements, since its abundance determination is generally more reliable than that of Sr and Zr. To avoid the stars whose Y abundances include s-process contributions, we select halo stars that satisfy $[Fe/H] < -2$ and $[Ba/Eu] < 0$. The $[Y/Eu]$ vs. $[Eu/Fe]$ diagram thus obtained is shown in Figure 2. The overall correlation between $[Y/Eu]$ and $[Eu/Fe]$ is summarized as (i) a decreasing $[Y/Eu]$ with increasing $[Eu/Fe]$ for $[Eu/Fe] \lesssim +1$ and (ii) a broadly constant $[Y/Eu]$ for $[Eu/Fe] \gtrsim +1$. Thus, r-II stars give the lowest $[Y/Eu]$ (≈ -1.1).

In this section, we argue that this observed correlation may be naturally explained by assuming that variations in both $[Eu/Fe]$ and $[Y/Eu]$ for metal-poor halo stars reflect directly those in nucleosynthesis from the merger

events. Specifically, the correlation between $[Y/Eu]$ and $[Eu/Fe]$ is regarded as the result of variations in the properties of cNSNSs or cBHNSs, for which Eu and Y are assumed to be synthesized separately in the tidal and non-tidal ejecta of individual merger events, respectively, as discussed in §2. Here, we assume the solar r-process pattern including the $A \sim 130$ peak (i.e., $Z \geq 52$) with no production for $Z < 52$ for the matter within the tidal ejecta from both cNSNSs and cBHNSs. On the other hand, for the non-tidal ejecta, we assume the nucleosynthesis pattern following the recent numerical results for the postmerger ejecta which show significantly low production of lanthanide elements and give the mass fraction of 1.64×10^{-2} for Y (Fujibayashi et al. 2018).

We first propose that the degree of Eu enhancement indicated by $[Eu/Fe]$ for individual stars ($-0.7 \lesssim [Eu/Fe] \lesssim +2$) could be basically determined by the different levels of Eu enrichment of gas via associated merger events (cNSNSs or cBHNSs) with widely varying masses (M_{tid}) of tidally-driven dynamical ejecta ($10^{-4} M_{\odot} \lesssim M_{\text{tid}} \lesssim 0.1 M_{\odot}$). Considering the $[Eu/Fe]$ distribution of halo stars, we identify two components: a Gaussian distribution in the range of $-0.7 \lesssim [Eu/Fe] \lesssim +1.3$ with a peak around $[Eu/Fe] \approx +0.3$ and an extending Eu-rich tail up to $[Eu/Fe] \approx +2$. Then, considering the predicted mass range of dynamical ejecta, cNSNS and cBHNS are likely to be responsible for producing the former and latter distributions, respectively. Approximate mass values of the mass of tidally-driven dynamical ejecta are shown in the upper part of the figure, implying that the average value $\langle M_{\text{tid}} \rangle$ for cNSNSs should be a few times $10^{-3} M_{\odot}$. If cBHNS should produce more Eu than cNSNS due to larger tidal mass ejection, the Y/Eu plateau could be connected to such events. Considering very low production of light r-process elements in the tidally dominated dynamical ejecta of cBHNSs owing to a low Y_e ($\lesssim 0.1$) (Roberts et al. 2017), we argue that Y in r-II stars originates from the postmerger ejecta.

The Y/Eu plateau implies that the production ratio of Y to Eu is quite similar in individual cBHNS events. Since each element owes its origin to non-tidal postmerger ejecta and tidally-driven dynamical ejecta, respectively, the masses of the two type of ejecta are suggested to scale linearly with each other. This linearity may also hold even if the postmerger ejecta of cBHNSs produce Eu due to a smaller Y_e resulting from lower neutrino irradiation (Fernández et al. 2017), though there are complexities in the influence of the neutrino treatment (e.g., Caballero et al. 2012; Wu et al. 2017). The required condition of a similar mass ratio of light r-process elements to Eu among the post-

merger ejecta of cBHNSs needs to be investigated (see also [Kyutoku et al. 2015](#)).

On the other hand, the trend of an increasing $[Y/Eu]$ with decreasing $[Eu/Fe]$ at the low $[Eu/Fe]$ regime is likely to reflect the diversity of nucleosynthesis in cNSNSs with various mass asymmetry in our scheme. The tidal interaction tends to be efficient for asymmetric binaries, and M_{tid} becomes large. At the same time, shock interactions are not very efficient for dynamical mass ejection in asymmetric binaries. Thus, the average values of Y_e become lower for more asymmetric binaries (e.g., [Sekiguchi et al. 2016](#)). These combined effects could explain the observed Y/Eu trend. According to this view, cNSNSs with massive ($\gtrsim 0.01M_{\odot}$) tidally-driven dynamical ejecta produce a very small amount of Y and share the Y/Eu plateau with cBHNSs. However, it is necessary to comprehensively investigate the dependence of nucleosynthesis in cNSNSs on the mass asymmetry and other binary parameters ([Kiuchi et al. 2019](#)), particularly in light of recently discovered highly asymmetric double NSs ([Ferdman et al. 2018](#)). In addition to the above discussion, a contrast in $[Y/Eu]$ may, in part, be attributed to the dependence of Y nucleosynthesis in the postmerger ejecta on their different masses. As one possibility, we anticipate that massive postmerger ejecta associated with massive dynamical ejecta produce a smaller amount of Y as a result of low Y_e , which is realized by a lower neutrino flux in accordance with a short timescale for collapsing into BHs. We also note that there still exists a downward trend for $[Y/Eu]$ with increasing $[Eu/H]$, which might support that Y production is connected to an Eu production site instead of being correlated with Fe production as predicted by LEPP ([Travaglio et al. 2004](#); [Montes et al. 2007](#)).

In our scheme, r-II stars are interpreted to be born from gas enriched by tidally-driven dynamical ejecta having very low Y_e , which result from either highly asymmetric double NS systems or BH-NS binaries. In such highly neutron-rich ejecta, the Y_e distribution inside each ejecta is likely skewed to be so low that the mass fraction with very low Y_e (e.g., < 0.18) is, in some of them, high enough (e.g., $> 30\%$) to induce a boost of actinide production ([Holmbeck et al. 2019](#)). This is consistent with the observed fact that among Th-measured halo stars, r-II stars include actinide-boost stars with higher fraction ($\sim 45\%$) than that ($\sim 25\%$) of less Eu -enhanced stars ($r\text{-I: } +0.3 \leq [Eu/Fe] < +1$) ([Holmbeck et al. 2018](#)). These arguments point to the r-II star's origin which could demand a specific nucleosynthesis condition rather than the properties such as a mass-scale of protogalaxies (clouds) where these stars originally resided.

4. CHEMICAL EVOLUTION OF R-PROCESS IN THE GALACTIC HALO

Chemical evolution study to explain an extensive scatter in $[Eu/Fe]$ among Galactic halo stars utilizing cNSNSs has been implemented by many authors (e.g., [Aragast et al. 2004](#); [van de Voort et al. 2015](#); [Shen et al. 2015](#); [Hirai et al. 2015, 2017](#)). The driver of a large scatter in these simulations is local inhomogeneities which can be produced when the limited amounts of interstellar matter are polluted by and mixed with the ejecta of each merger event occurring with a low frequency: inhomogeneous mixing could produce larger $[Eu/Fe]$ in strongly polluted areas and smaller values in less polluted ones. On the other hand, our scheme predicts that the variation in $[Eu/Fe]$ among halo stars is primarily caused by the different masses of tidally-driven dynamical ejecta from cNSNSs and cBHNSs. To validate this hypothesis, we model the chemical evolution of the Galactic halo and calculate the Eu/Fe evolution.

We consider protogalactic fragments with a baryonic mass of 10^6M_{\odot} , which is the minimum baryonic mass at the epoch of galaxy formation ([Tegmark et al. 1997](#)). This fragment mass is also implied from the threshold of an initial mass of protogalaxies, as implied from Ret II. The observed $[Eu/H] \approx -1$ of r-II stars in this galaxy implies that an Eu mass ejected from a cNSNS with $M_{\text{tid}} \approx 0.01M_{\odot}$ is mixed with gas having a mass of $\sim 10^6M_{\odot}$ (see also [Ji et al. 2015, 2016](#)). In each fragment, separate chemical evolutions proceed as building blocks of the halo. Thus, metal-poor stars in the Galaxy are predicted to be an assembly of stars originating from individual fragments, according to the hierarchical galaxy formation scheme. This scenario does not distinguish whether each fragment corresponds to an accreted unit of the Galaxy or one of many pieces of an accreted massive dwarf galaxy, such as Gaia-Enceladus ([Helmi et al. 2018](#)). In fragments, the ejecta are considered to propagate inside the whole volume and thus are well-mixed. This is justified by both a broad uniformity of Eu abundances in Ret II ([Ji et al. 2016](#)) and the abundance of ^{244}Pu in the solar vicinity, which suggests that the ejecta of cNSNSs are mixed with local gas as massive as $\gtrsim 10^6M_{\odot}$ ([Tsujimoto et al. 2017b](#)).

In each fragment, star formation is assumed to continue for a duration of 300 Myr at a low star formation rate so as to give $\langle [Fe/H] \rangle \approx -1.6$ as observed for halo stars, which results in a conversion of about 17% of gas to stars. Owing to the short duration considered here, the contribution of Fe from type Ia SNe is not included. For Fe yields from CCSNe, we assume the nucleosynthesis yields tabulated in [Kobayashi et al. \(2006\)](#). We

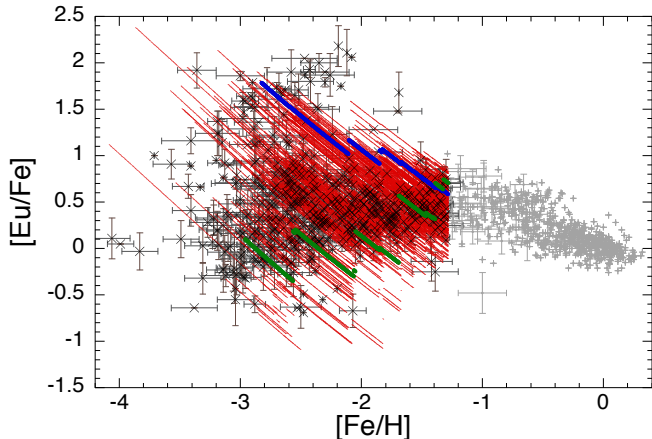


Figure 3. Predicted $[\text{Eu}/\text{Fe}]-[\text{Fe}/\text{H}]$ correlations for the Galactic halo (red lines) compared with the observed data (crosses). For reference, the data of mainly disk stars for $[\text{Fe}/\text{H}] > -1.3$ are shown by small pluses. Predicted feature is the assembly of 100 randomly selected cases for the chemical evolution in protogalactic fragments with a mass of $10^6 M_{\odot}$. Among them, two representative evolutionary paths are highlighted by green and blue lines (see the text).

assume that an Eu ejection occurs at a rate of one per ~ 200 CCSNe (see §4.1), which leads to ~ 6 events in total. For each event, the ejected mass of Eu is given by randomly assigning the mass of tidally-driven dynamical ejecta from $10^{-4} M_{\odot}$ to $0.07 M_{\odot}$, with a Gaussian probability distribution having a peak at $3 \times 10^{-3} M_{\odot}$ for $M_{\text{tid}} \leq 0.01 M_{\odot}$. For $M_{\text{tid}} \geq 0.01 M_{\odot}$, we assign a 10% probability in total with uniform mass distribution. Then, the Eu mass ejected from each merger event is calculated from M_{tid} composed of r-process elements with $Z \geq 52$ following the solar r-process pattern. For the delay time of the ejection of r-process elements, we adopt a short timescale of 10 – 30 Myr to accelerate the early r-process enrichment in the halo (Tsujiimoto & Shigeyama 2014b).

Since a sequence of r-process events occurs with randomly chosen masses of tidally-driven dynamical ejecta, individual evolutionary paths of Eu/Fe vary among protogalactic fragments. Figure 3 shows a mixture of such paths in 100 fragments. They include two examples that largely differ in Eu production by tidally-driven dynamical ejecta (distinguished by different colors): an initial Eu-boost making r-II stars, followed by a decreasing trend of $[\text{Eu}/\text{Fe}]$ (blue), and a gradual increase in $[\text{Eu}/\text{Fe}]$ via a sequence of mild Eu-enrichment by each event, resulting in no r-II stars (green). This figure excludes the initial generations of stars with no Eu content. It shows broad agreement between our predicted feature and the observation. On the other hand, if we adopt the delay time distribution for the merger ob-

jects spanning over gigayears implied from that for short gamma-ray bursts (Fong et al. 2017), there is a poorer agreement with the observation mainly due to a smaller predicted scatter in $[\text{Eu}/\text{Fe}]$ by a reduced number of r-process events within a short duration (300 Myr) of star formation. Note that Eu abundance in disk stars favors a primary r-process production with a short time delay over long-delay merger events (e.g., Côté et al. 2019; Siegel et al. 2019; Lin et al. 2019). Accordingly, we claim that the large scatter in the abundance ratio that is unique to r-process elements in the Galactic halo is an end result of r-process enrichment driven by merger events under halo formation via mass assembly of small building blocks. In these merger events, widely spanning masses of tidally-driven dynamical ejecta are realized.

5. MERGER EVENT RATE

Based on our proposed scheme, we can discuss the event rates of cNSNSs and cBHNSs associated with r-process production. On the other hand, Advanced LIGO/Virgo Observing Runs 1 and 2 by the ongoing gravitational-wave search project give the reliable rates of cNSNSs and cBHNSs (The LIGO Scientific Collaboration et al. 2018). Thus, the comparison between the two results will help to verify our argument presented here. In general, the assessment of merger event rates from the analysis of r-process abundance assuming the connection of r-process production with the merger events is highly uncertain unless a mean ejecta mass is narrowed down (Rosswog et al. 2017; Hotokezaka et al. 2018). Our scheme that assigns each (tidal) ejecta mass to each $[\text{Eu}/\text{Fe}]$ ratio of Galactic halo stars could give a one possible way to resolve this problem through a statistical treatment.

5.1. NS-NS

First, we estimate the cNSNS event rate in the local volume (LV) of the Universe, R_{LV} . This can be directly compared with the rate deduced from gravitational-wave events in the local Universe. R_{LV} can be converted from the present rate for the Galaxy, R_{G} , which is obtained through an analysis of stellar r-process abundances combined with the recent star formation activity in the Galaxy (Tsujiimoto & Shigeyama 2014b; Tsujiimoto et al. 2017b). Note that R_{G} would be lower than the mean rate for the Galaxy (Rosswog et al. 2017; Hotokezaka et al. 2018) owing to the currently low star formation rate (e.g., Mor et al. 2019), and this tendency of star formation seen in the Galaxy is shared with M31 (Bernard et al. 2015). In this study, we utilize the most reliably measured stellar abundance: the solar abundance.

The key point is that the relative solar abundance ratio of Eu to Mg (5.2×10^{-7}) is equivalent to the relative nucleosynthesis yield between the two elements. Here the Eu yield is defined per CCSN basis, that is, as the combination of the Eu mass per cNSNS event and a reciprocal number of CCSNe that is necessary to give birth to one cNSNS event. For the Mg yield from a single CCSN, we adopt a mass of $0.1 M_{\odot}$. This value is deduced from two arguments: (i) nucleosynthesis calculations for CCSNe give $0.1-0.125 M_{\odot}$ as an IMF-weighted average Mg mass for the progenitor's mass range of $13-50 M_{\odot}$ (Tominaga et al. 2007) and (ii) a relative yield with a mean Fe mass of $\sim 0.07 M_{\odot}$ obtained from a light curve analysis of CCSNe (Hamuy 2003) leads to an observed plateau of $[\text{Mg}/\text{Fe}] \approx +0.4$ among halo stars and thus the value of the most metal-poor disk stars (e.g., Bensby et al. 2014). Accordingly, we obtain the Eu yield of $5.2 \times 10^{-8} M_{\odot}$.

Then, this together with an average Eu mass per cNSNS event leads to the cNSNS rate. The Eu mass fraction of 6×10^{-3} in the tidally-driven dynamical ejecta, which is obtained from the assumption of the solar r-process pattern for the elements with $Z \geq 52$, provides the cNSNS rate per CCSNe of one per $1150 \langle M_{\text{tid}} \rangle / 0.01 M_{\odot}$ CCSNe. This further leads to the Galactic cNSNS rate R_{G} , using the present-day Galactic CCSN rate of 2.3 SNe per century (Li et al. 2011):

$$R_{\text{G}} \approx 20 \left(\frac{\langle M_{\text{tid}} \rangle}{0.01 M_{\odot}} \right)^{-1} \text{ Myr}^{-1}. \quad (1)$$

Finally, this rate can be converted to the rate for the local volume of the Universe via the density of a Milky Way-equivalent galaxy of $1.16 \times 10^{-2} \text{ Mpc}^{-3}$ estimated from the blue luminosity (Abadie et al. 2010):

$$R_{\text{LV}} \approx 230 \left(\frac{\langle M_{\text{tid}} \rangle}{0.01 M_{\odot}} \right)^{-1} \text{ Gpc}^{-3} \text{ yr}^{-1}. \quad (2)$$

This R_{LV} range is within the rate at the 90% confidence intervals of $110-3840 \text{ Gpc}^{-3} \text{ yr}^{-1}$, with the most probable value around $\sim 1000 \text{ Gpc}^{-3} \text{ yr}^{-1}$ by gravitational-wave detection (The LIGO Scientific Collaboration et al. 2018). Therefore, R_{LV} deduced from the solar abundance is in agreement with that from the gravitational-wave event rate if the average mass of tidally-driven dynamical ejecta is assumed to be a few times $10^{-3} M_{\odot}$.

5.2. BH-NS producing r-process elements

The cBHNSs events associated with r-process production are considered rare among all cBHNSs (Zappa et al. 2019) whose event rate is constrained to be $< 610 \text{ Gpc}^{-3} \text{ yr}^{-1}$ (The LIGO Scientific Collaboration et al.

2018). We can predict the approximate rate based on our theoretical scheme that the group of stars enriched by the r-process to the highest level ($[\text{Eu}/\text{Fe}] \gtrsim +1.4$) can be connected to a cBHNS origin, while other stars are associated with a cNSNS origin. The fraction of r-II stars compared to all metal-poor halo stars is estimated to be about 2–4%, although this estimate likely overrepresents due to incomplete sampling (Brauer et al. 2019). Then, considering that the fraction of r-II stars with $[\text{Eu}/\text{Fe}] \geq +1.4$ with respect to all r-II stars is about 25% (10/38: Roederer et al. 2018), the event ratio of cBHNSs producing r-process elements to cNSNSs is implied to be about 0.5–1% at maximum. Accordingly, we anticipate that the future detection of the gravitational-wave events originating from cBHNSs could be inclined towards no association with electromagnetic counterparts. If we adopt $1000 \text{ Gpc}^{-3} \text{ yr}^{-1}$ as a fiducial value of the cNSNS event rate, the event rate of cBHNS with the r-process, a few per Gpc^3 per year, is deduced as the most likely case.

6. SUMMARY

We show that the large scatter in the $[\text{Eu}/\text{Fe}]$ ratio among Galactic halo stars can be the outcome of varying Eu production, spanning three orders of magnitude in the masses of tidally-driven dynamical ejecta from both cNSNSs and cBHNSs. The origin of r-II stars is predicted to have a close connection to a highly neutron-rich environment, which could be realized in the massive ($\sim 0.01-0.02 M_{\odot}$) dynamical ejecta from cNSNSs with highly asymmetric double NS systems or those from cBHNSs. On the other hand, enrichment by cNSNSs with less massive ejecta results in halo stars having an observed variation in the [light r-process/Eu] ratio with less enhancement in Eu. We further predict that the typical mass of tidally-driven dynamical ejecta for cNSNSs should be a few times $10^{-3} M_{\odot}$, which is nicely supported by the cNSNS rate deduced from the ongoing gravitational-wave observations.

Our scenario is based on the idea that the correlation between Y/Eu and Eu/Fe emerges from different neutron richness of the ejecta caused by different properties of coalescing binaries. Specifically, the amount of the neutron-rich tidal ejecta and the Eu yield are presumed to increase as the binary becomes asymmetric and tidal deformation of the lighter component is enhanced. Although this trend is consistent with the results of previous studies (e.g., Sekiguchi et al. 2016), whether the observed correlation is reproduced quantitatively should be investigated by future hydrodynamical simulations and nucleosynthetic calculations with systematically varying the binary parameters such as the

mass ratio. These inputs would help to promote a thorough understanding of Galactic elemental features for all r-process elements, including light r-process nuclei, lanthanides, and actinides.

The authors thank an anonymous referee for his or her valuable comments. This work was supported by JSPS

KAKENHI grant Nos. 16H06342, 17H01131, 18H01258, 18H04593, 18H04595, JP18H05236, and 19K14720, and MEXT Japan (“Priority Issue on Post-K computer: Elucidation of the Fundamental Laws and Evolution of the Universe”). NN thanks S. Fujibayashi for fruitful discussions on the post-merger ejecta.

REFERENCES

- Abadie, J., Abbott, B. P., Abbott, R., et al. 2010, *CQGra*, 27, 173001
- Abomalima, A., & Frebel, A. 2018, *ApJS*, 238, 36
- Allen, D. M., Ryan, S. G., Rossi, S., Beers, T. C., & Tsangarides, S. A. 2012, *A&A*, 548, A34
- Aoki, W., Honda, S., Beers, T. C., et al. 2005, *ApJ*, 632, 611
- Argast, D., Samland, M., Thielemann, F.-K., & Qian, Y.-Z. 2004, *A&A*, 416, 997
- Arcones, A., & Bliss, J. 2014, *J. Phys. G: Nucl. Phys.*, 41, 044005
- Bauswein, A., Goriely, S., & Janka, H.-T. 2013, *ApJ*, 773, 78
- Beers, T. C., & Christlieb, N. 2005, *ARA&A*, 43, 531
- Bensby, T., Feltzing, S., & Oey, M. S. 2014, *A&A*, 562, A71
- Bernard, E. J., Ferguson, A. M. N., Richardson, J. C., et al. 2015, *MNRAS*, 446, 2789
- Bisterzo, S., Travaglio, C., Gallino, R., Wiescher, M., & Käppeler, F. 2014, *ApJ*, 787, 10
- Bovard, L. D., Martin, F., Guercilena, F., Arcones, A., Rezzolla, L., & Korobkin, O. 2017, *PhRvD*, 96, 124005
- Brauer, K., Ji, A. P., Frebel, A., Dooley, G. A., Gómez, F. A., & O’Shea, B. W. 2019, *ApJ*, 871, 247
- Caballero, O. L., McLaughlin, G. C., & Surman, R. 2012, *ApJ*, 745, 170
- Côté, B., Fryer, C. L., Belczynski, K., et al. 2018, *ApJ*, 855, 99
- Côté, B., Eichler, M., Arcones, A., et al. 2019, *ApJ*, 875, 106
- Coulter, D. A., Foley, R. J., Kilpatrick, C. D., et al. 2017, *Science*, 358, 1556
- Cowan, J. J., Sneden, C., Lawler, J. E., et al. 2019, *arXiv:1901.01410*
- Cowperthwaite, P. S., Berger, E., Villar, V. A., et al. 2017, *ApJL*, 848, L17
- Eichler, M., Arcones, A., Kelic, A., et al. 2015, *ApJ*, 808, 30
- Farouqi, K., Kratz, K.-L., Pfeiffer, B., et al. 2010, *ApJ*, 712, 1359
- Ferdman, R. D., & PALFA Collaboration 2018, in *IAU Symposium*, Vol. 337, *Pulsar Astrophysics the Next Fifty Years*, ed. P. Weltevrede, B. B. P. Perera, L. L. Preston, & S. Sanidas, 146
- Fernández, R., Foucart, F., Kasen, D., Lippuner, J., Desai, D., & Roberts, L. F. 2017, *CQGra*, 34, 154001
- Fong, W., Berger, E., & Blanchard, P. K., et al. 2017, *ApJL*, 848, L23
- Foucart, F., O’Connor, E., Roberts, L., Kidder, L. E., Pfeiffer, H. P., & Scheel, M. A. 2016, *PhRvD*, 94, 123016
- François, P., Depagne, E., Hill, V., et al. 2007, *A&A*, 476, 935
- Freiburghaus, C., Rosswog, S., & Thielemann, F.-K. 1999, *ApJ*, 525, L121
- Frensel, M., Wu, M.-R., Volpe, C., & Perego, A. 2017, *PhRvD*, 95, 023011
- Fujibayashi, S., Kiuchi, K., Nishimura, N., Sekiguchi, Y., & Shibata, M. 2018, *ApJ*, 860, 64
- Fujimoto, S., Nishimura, N., & Hashimoto, M. 2008, *ApJ*, 680, 1350
- Goriely, S. 2015, *EPJA*, 51, 22
- Halevi, G., & Mösta, P. 2018, *MNRAS*, 477, 2366
- Hamuy, M. 2003, *ApJ*, 582, 905
- Helmi, A., Babusiaux, C., Koppelman, H. H., Massari, D., Veljanoski, J., & Brown, A. G. A. 2018, *Nature*, 563, 85
- Hirai, Y., Ishimaru, Y., Saitoh, T. R., Fujii, M. S., Hidaka, J., & Kajino, T. 2015, *ApJ*, 814, 41
- Hirai, Y., Ishimaru, Y., Saitoh, T. R., Fujii, M. S., Hidaka, J., & Kajino, T. 2015, *MNRAS*, 466, 2474
- Holmbeck, E. M., Beers, T. C., Roederer, I. U., et al. 2018, *ApJL*, 859, L24
- Holmbeck, E. M., Frebel, A., McLaughlin, G. C., Mumpower, M. R., Sprouse, T. M., & Surman, R. 2019, *ApJ*, 881, 5
- Hotokezaka, K., Beniamini, P., & Piran, T. 2018, *IJMPD*, 27, 1842005
- Hotokezaka, K., Kiuchi, K., Kyutoku, K., Okawa, H., Sekiguchi, Y., Shibata, M., & Taniguchi, K. 2013, *PhRvD*, 88, 044026
- Ji, A. P., Frebel, A., & Bromm, V. 2015, *MNRAS*, 454, 659

- Ji, A. P., Frebel, A., Chiti, A., & Simon, J. D. 2016, *Nature*, 531, 610
- Just, O., Bauswein, A., Adrevo Pulpillo, R., Goriely, S., & Janka, H.-T. 2015, *MNRAS*, 448, 541
- Kitaura, F. S., Janka, H.-Th, & Hillebrandt, W. 2006, *A&A*, 450, 345
- Kiuchi, K., Kyutoku, K., Shibata, M., & Taniguchi, K. 2019, *ApJL*, 876, L31
- Kobayashi, C., Umeda, H., Nomoto, K., Tominaga, N., & Ohkubo, T. 2006, *ApJ*, 653, 1145
- Kyutoku, K., Ioka, K., Okawa, H., Shibata, M., & Taniguchi, K. 2015, *PhRvD*, 92, 044028
- Li, W., Chornock, R., Leaman, J., et al. 2011, *MNRAS*, 412, 1473
- Lin, J., Asplund, M., Ting, Y.-S., et al. 2019, *arXiv:1911.05221*
- Lippuner, J., Fernández, R., Roberts, L. F., et al. 2017, *MNRAS*, 472, 904
- Macias, P., & Ramirez-Ruiz, E. 2019, *ApJL*, 877, L24
- MacFadyen, A. I., & Woosley, S. E. 1999, *ApJ*, 524, 262
- Malkus, A., McLaughlin, G. C., & Surman, R. 2016, *PhRvD*, 93, 045021
- Mashonkina, L., Christlieb, N., & Eriksson, K. 2014, *A&A*, 569, A43
- Mendoza-Temis, J. J., Wu, M.-R., Langanke, K., Martínez-Pinedo, G., Bauswein, A., & Janka, H.-T. 2015, *PhRvC*, 92, 055805
- Metzger, B. D., & Fernández, R. 2014, *MNRAS*, 441, 3444
- Montes, F., Beers, T. C., Cowan, J. J., et al. 2007, *ApJ*, 671, 1685
- Mor, R., Robin, A. C., Figueras, F., Roca-Fàbrega, S., & Luri, X. 2019, *A&A*, 624, L1
- Mösta, P., Roberts, L. F., Halevi, G., Ott, C. D., Lippuner, J., Haas, R., & Schnetter, E. 2018, *ApJ*, 864, 171
- Pian, E., D'Avanzo, P., Benetti, S., et al. 2017, *Nature*, 551, 67
- Nishimura, N., Takiwaki, T., & Thielemann, F.-K. 2015, *ApJ*, 810, 109
- Nishimura, N., Podolyák, Z., Fang, D.-L., & Suzuki, T. 2016, *PhLB*, 756, 273
- Nishimura, N., Sawai, H., Takiwaki, T., Yamada, S., & Thielemann, F.-K. 2017, *ApJL*, 836, L21
- Qian, Y.-Z., & Wasserburg, G. J. 2007, *Phys. Rep.*, 444, 237
- Radice, D., Perego, A., Hotokezaka, K., Fromm, S. A., Bernuzzi, S., & Roberts, L. F. 2018, *ApJ*, 869, 130
- Roberts, L. F., Lippuner, J., Duez, M. D., et al. 2017, *MNRAS*, 464, 3907
- Roederer, I. U., Hattori, K., & Valluri, M. 2018, *AJ*, 156, 179
- Rosswog, S., Feindt, U., Korobkin, O. et al. 2017, *CQGra*, 34, 104001
- Sakari, C. M., Placco, V. M., Hansen, T., et al. 2018, *ApJL*, 854, L20
- Sekiguchi, Y., Kiuchi, K., Kyutoku, K., & Shibata, M. 2015, *PhRvD*, 91, 064059
- Sekiguchi, Y., Kiuchi, K., Kyutoku, K., Shibata, M., & Taniguchi, K. 2016, *PhRvD*, 93, 124046
- Shen, S., Cooke, R. J., Ramirez-Ruiz, E., Madau, P., Mayer, L., & Guedes, J. 2015, *ApJ*, 807, 115
- Siegel, D. M., & Metzger, B. D. *ApJ*, 858, 52
- Siegel, D. M., Barnes, J., & Metzger, B. D. 2019, *Nature*, 569, 241
- Simmerer, J., Sneden, C., Cowan, J., Collier, J., Woolf, V. M., & Lawler, J. E. 2004, *ApJ*, 617, 1091
- Smartt, S. J., Chen, T.-W., Jerkstrand, A., et al. 2017, *Nature*, 551, 75
- Sneden, C., Preston, G. W., McWilliam, A., & Searle, L. 1994, *ApJL*, 431, L27
- Suda, T., Katsuya, Y., Yamada, S., et al. 2008, *PASJ*, 60, 1159
- Tegmark, M., Silk, J., Rees, M. J., Blanchard, A., Abel, T., & Palla, F. 1997, *ApJ*, 474, 1
- The LIGO Scientific Collaboration, the Virgo Collaboration, Abbott, B. P., et al. 2018, *arXiv:1811.12907*
- Thielemann, F.-K., Eichler, M., Panov, I. V., & Wehmeyer, B. 2017, *ARNPS*, 67, 253
- Tian, J. Y., Patwardhan, A. V., & Fuller, G. M. 2017, *PhRvD*, 96, 043001
- Tominaga, N., Umeda, H., & Nomoto, K. 2007, *ApJ*, 660, 516
- Travaglio, C., Gallino, R., Arnone, E., Cowan, J. J., Jordan, F., & Sneden, C. 2004, *ApJ*, 601, 864
- Tsujimoto, T., & Shigeyama, T. 2014a, *ApJL*, 795, L18
- Tsujimoto, T., & Shigeyama, T. 2014b, *A&A*, 565, L5
- Tsujimoto, T., Matsuno, T., Aoki, W., Ishigaki, M. N., & Shigeyama, T. 2017a, *ApJL*, 850, L12
- Tsujimoto, T., Yokoyama, T., & Bekki, K. 2017b, *ApJL*, 835, L3
- van de Voort, F., Quataert, E., Hopkins, P. F., Kereš, D., Faucher-Giguère, C.-A. 2015, *MNRAS*, 447, 140
- Vassh, N., Vogt, R., Surman, R., et al. 2019, *JPhG*, 46, 065202
- Vincent, T., Foucart, F., Duez, M. D., et al. 2019, *arXiv:1908.00655*
- Wanajo, S. 2018, *ApJ*, 868, 65
- Wanajo, S., Janka, H.-T., & Müller, B. 2011, *ApJL*, 726, L15

- Wanajo, S., Sekiguchi, Y., Nishimura, N., Kiuchi, K., Kyutoku, K., & Shibata, M. 2014, *ApJL*, 789, L39
- Watson, D., Hansen, C. J., Selsing, J., et al. 2019, *Nature*, 574, 497
- Wehmeyer, B., Pignatari, M., & Thielemann, F.-K. 2015, *MNRAS*, 452, 1970
- Wehmeyer, B., Frohlich, C., Côteé, B., Pignatari, M., & Thielemann, F.-K. 2019, *MNRAS*, 487, 1745
- Winteler, C., Käppeli, R., Perego, A., et al. 2012, *ApJ*, 750, L22
- Wu, M.-R., Tamborra, I., Just, O., & Janka, H.-T. 2017, *PhRvD*, 96, 123015
- Zappa, F., Bernuzzi, S., Pannarale, F., Mapelli, M., & Giacobbo, N. 2019, *PhRv Lett.*, 123, 041102